Author/s:
Cho, I;Kendrick, WJ;Stuart, AN;Ramkissoon, P;Ghiggino, KP;Wong, WWH;Lakhwani, G

Title:
Multi-resonance TADF in optical cavities: suppressing excimer emission through efficient energy transfer to the lower polariton states

Date:
2023-10-26

Citation:
Cho, I., Kendrick, W. J., Stuart, A. N., Ramkissoon, P., Ghiggino, K. P., Wong, W. W. H. & Lakhwani, G. (2023). Multi-resonance TADF in optical cavities: suppressing excimer emission through efficient energy transfer to the lower polariton states. Journal of Materials Chemistry C, 11 (41), pp.14448-14455. https://doi.org/10.1039/d3tc02133e.

Journal of
Materials Chemistry C

Materials for optical, magnetic and electronic devices

Accepted Manuscript

This article can be cited before page numbers have been issued, to do this please use: I. Cho, W. J. Kendrick, A. N. Stuart, P. Ramkissoon, K. Ghiggino, W. W. H. Wong and G. Lakhwani, *J. Mater. Chem. C*, 2023, DOI: 10.1039/D3TC02133E.

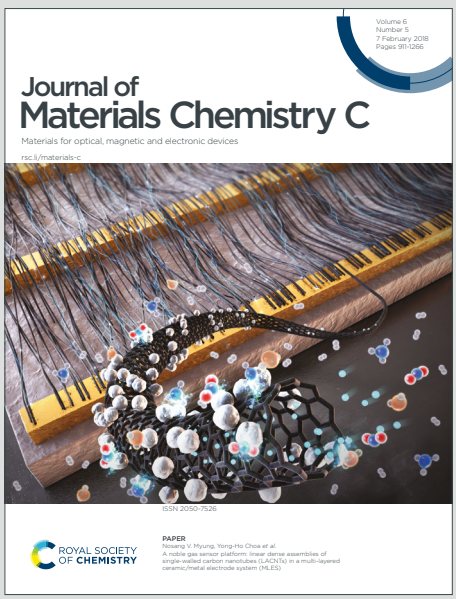

ROYAL SOCIETY OF CHEMISTRY

rsc.li/materials-c

Multi-resonance TADF in optical cavities: Supressing excimer emission through efficient energy transfer to the lower polariton states

Inseong Cho,[a] William J. Kendrick,[b] Alexandra N. Stuart,[a] Pria Ramkissoon,[b] Kenneth P. Ghiggino,[b] Wallace W. H. Wong,[b] and Girish Lakhwani*[,a,c]

[a]*ARC Centre of Excellence in Exciton Science, School of Chemistry, The University of Sydney, NSW 2006, Australia*

[b]*ARC Centre of Excellence in Exciton Science, School of Chemistry, The University of Melbourne, Parkville, VIC 3010, Australia*

[c]*The University of Sydney Nano Institute, Sydney NSW 2006, Australia*

Email address: girish.lakhwani@sydney.edu.au

ABSTRACT: Thermally activated delayed fluorescence (TADF) emitters suffer from molecular aggregation that limits their applicability in light emitting devices. Aggregation-induced excimer formation often leads to a larger Stokes shift, broader emission spectrum, and reduced emission quantum yields, limiting emitter dye loading to a few weight percent in organic light emitting devices. Here, we demonstrate suppression of excimer emission by dispersing a synthesised multi resonance TADF emitter dye (OQAO(mes)$_2$) in a PMMA host matrix and embedding the host-guest photoactive layer into an optical cavity. Rabi splitting up to 0.24 eV is obtained at 35 wt.% dye loading. Under the strong coupling regime, prompt and delayed emission through excimer states is suppressed due to efficient energy transfer to the lower polariton (LP) states, demonstrated by the blue shift of the emission spectrum and narrowing of the emission linewidth. We also observe an increase in reverse intersystem (RISC) rate constants up to 33% that we attribute to a decrease in activation energy by ≈2 kT. This work highlights that strong light-matter interactions can be exploited to overcome aggregation-induced excimer losses providing a pathway towards efficient organic light-emitting diodes with high colour purity and organic semiconductor polariton lasing.

INTRODUCTION

Triplet formation is a loss pathway in organic light emitting diodes (OLEDs) due to the weakly emissive nature and the long lifetime of triplet excitons leading to triplet-polaron quenching and triplet-triplet annihilation.[1-6] Recently, thermally activated delayed fluorescence (TADF) has attracted great attention due to its ability to harvest triplet excitons back into bright singlet excitons by thermal energy through reverse intersystem crossing (RISC). Traditionally, TADF molecules are designed with reduced spatial overlap between wavefunctions of the HOMO and the LUMO, which results in the energy gap between low lying singlet (S_1) and triplet (T_1) states (ΔE_{ST}) being significantly lower (typically < 0.2 eV) than that commonly observed in organic chromophores (0.5-1.0 eV).[7] Such a low ΔE_{ST} enables facile RISC by using surrounding thermal energy, through which light is emitted as delayed fluorescence within the time scales of a few μs.[8] However, the small overlap between the electron and the hole densities on the HOMO and the LUMO often leads to low oscillator strength of orbital transitions which makes it difficult to present both small ΔE_{ST} and high quantum yield.[9] Moreover, the structural relaxation in the excited states leads to broad emission bandwidth and a large Stokes shift, which limits colour purity of OLEDs.[9, 10]

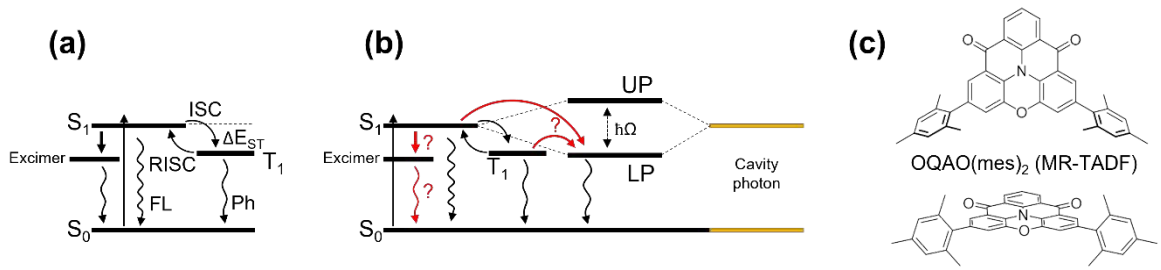

Figure 1. (a) Energy diagram of TADF and (b) that in an optical cavity, and (c) chemical structure of OQAO(mes)$_2$ (front (top) and side (bottom) views). ISC is the intersystem crossing, RISC is the reverse intersystem crossing, FL is the fluorescence, and Ph is the phosphorescence, UP is the upper polariton, LP is the lower polariton, and Ω is the Rabi splitting.

Multi-resonance TADF (MR-TADF) emitters have emerged as promising fluorescence emitters for next generation OLEDs and organic semiconductor lasing.[10-12] Adequate separation between electrons and holes localised on the HOMO and the LUMO that are alternatively placed on different atoms of

polycyclic rings allows high oscillator strength while keeping small ΔE_{ST}.[9] Furthermore, the rigid structure along with the alternating electron density distribution reduces structural relaxation and vibronic coupling between S_1 and S_0, resulting in sharp emission bandwidth with small Stokes shifts.[9, 13, 14] However, the planar structures of the MR-TADF dye molecules often lead to strong intermolecular π- π interactions,[15] causing molecular aggregation that leads to thermalisation losses and bimolecular quenching of triplets at high concentrations/fluence, which limits doping concentrations of dye molecules in a polymer host matrix to a few weight percents (typically < 5 wt.%).[14, 16-18] Furthermore, formation of an excimer – a transient dimer formed between an excited molecule and a molecule in its ground state – causes emission linewidth broadening and red-shift of emission due to its lower lying energy compared to that of the molecularly isolated dyes (Figure 1a).[19-22] This is undesirable in light emitting applications as it can reduce the colour purity of the system.

For TADF molecules to be efficient in OLEDs or lasing applications, the rate constant of RISC (k_{RISC}) should be fast enough to compete with alternate triplet loss pathways.[23] k_{RISC} can be increased with smaller ΔE_{ST}.[12, 24] This relationship was also demonstrated by Aizawa *et al.* via inverting S_1 and T_1.[25] They showed negative ΔE_{ST} in trifluoro-ethyl-substituted heptazine-based molecule under double excitation where k_{RISC} was enhanced two-fold compared to the molecular analogue with positive ΔE_{ST}. However, changing molecular structure can bring other complexities such as solubility, intermolecular interactions and altered energetics.

Alternatively, the exciton energy landscape can be altered without changing molecular structure via strong light-matter interactions. Strong light-matter coupling is an interaction between an excitonic transition of an organic molecule and a resonating photon mode inside an optical cavity, forming hybrid half-light half-matter quasi-particles called polaritons (see Figure 1b and 3c). Under the strong coupling regime, two quasi-energy states; upper and lower polaritons (UP and LP, respectively) are formed and the magnitude of the split is quantified as Rabi-splitting (Ω).[26] Due to their photonic nature, polaritons are delocalised over a long range in a medium[27, 28] therefore energy transfer becomes more

efficient, enabling a long-range energy transport in the system.[29-31] In 2018, Stranius *et al.* demonstrated that RISC can be enhanced in a fluorone-based phosphoric molecule (ΔE_{ST}=0.426 eV) under strong coupling. They showed reduction in the activation energy (E_a) of the phosphor by 0.12 eV in optical microcavities whereby triplets can effectively be recycled to the LP state.[32] In another study, Eizner *et al.* reported that, by embedding a trigonal donor-acceptor type TADF emitter that has ΔE_{ST} of 0.1 eV in an optical cavity, they found that LP states lie below T_1 energy states.[33] However, changes observed in the RISC rate were negligible regardless of the degree of Rabi splitting, which they attributed to delayed fluorescence mediated predominately from dark states due to a very large number of uncoupled molecules in the neat photoactive layer. In 2021, Yu *et al.* showed that LP state energy can be tuned by tuning photon energy in optical cavities, demonstrating that k_{RISC} for the vacuum deposited MR-TADF system was independent of the temperature due to activation-less RISC to the LP state lying below the triplet energy state.[34] The same group also reported that delayed emission from excimeric states in a MR-TADF emitter can be mitigated in optical cavities, via excimer to LP transition.[35] However, the relationship between exciton transition pathways/dynamics and the degree of strong coupling in TADF emitters with molecular aggregation and excimer formation as shown in Figure 1b has not been clearly demonstrated. Here, we show that under strong coupling emission through excimer states is suppressed due to efficient energy transfer and RISC to the LP states, demonstrated by the blue shifted emission spectrum and narrower emission linewidth. Furthermore, it is observed that k_{RISC} enhances in the cavities by up to 33% due to RISC to the LP states.

To achieve strong light matter coupling, exchange interactions between optical fields in a cavity and excitonic transition must be faster than any loss mechanism, such as thermalisation. General material requirements are large oscillator strengths and narrow absorption linewidths.[36] Rabi splitting is proportional to the number of molecules coupled to the cavity photon mode, hence high dye loading in the cavity is beneficial but not at the cost of aggregation-induced thermalisation losses.[32, 37] We synthesised and employed a mesityl-substituted fused-triphenyl amine (2,6-dimesitylbenzo[9,1]quinolizino[3,4,5,6,7-*klmn*]phenoxazine-8,12-dione, $OQAO(mes)_2$) as a MR-TADF

View Article Online
DOI: 10.1039/D3TC02133E

emitter for strong light-matter interactions (see Figure 1c). A molecular analogue, OQAO has previously been reported as a MR-TADF for OLEDs with large oscillator strength, sharp absorption and emission band widths, small Stokes shift, and high quantum yield of 90.2% in a diluted toluene solution.[38] However, loading remained low at 5 wt.% in the host material, and the film was fabricated by a vacuum deposition method. To enable high dye loading in a solution-processed host matrix, we added bulky mesityl groups to the OQAO scaffold. ΔE_{ST} of OQAO(mes)$_2$ 0.15 eV was found to be close to that of the unsubstituted OQAO (0.16 eV) reported by Zou *et al*.[38] Angle-resolved reflection and emission measurements of OQAO(mes)$_2$ in optical cavities revealed Ω of up to 0.24 eV at high 35 wt.% doping concentration and emission predominantly originating from LP stats. Photoluminescence lifetime measurements showed that k_{RISC} is enhanced in optical cavities due to lower E_a of RISC to the LP states. We found that the formation of polaritons efficiently suppresses excimer emission due to efficient energy transfer to the LP states.

RESULTS AND DISCUSSION

Optical Properties of OQAO(mes)$_2$ films.

We first measured the optical properties of OQAO(mes)$_2$ as a function of concentration in a PMMA matrix (2.4, 4.8, 9.1, and 35 wt.%) (see Figure S1 in the supporting information, SI). Absorption of the films was slightly red-shifted from 500 to 507 nm with increasing concentration. The emission was more significantly red-shifted from 535 nm at 2.4 wt.% to 560 nm at 35 wt.% and exhibited increased shoulder emission at higher doping concentrations (Figure 2a and S1). The red-shifted emission with increasing doping concentration indicates molecular aggregation which stabilises singlet states to a lower energy. The increased emission shoulder at the higher concentrations was attributed to excimer emission (see deconvoluted spectra in Figure S2). Note, optical density of the thin film was low (≈0.1) hence we can rule out the spectral shape changes being due to reabsorption (see Figure S3). As shown in Figure 2b, prompt and delayed emission are present, and the lifetime of the delayed emission increases at lower temperature. In addition, the intensity of the delayed emission at cryogenic

temperature is lower than that at room temperature. The temperature-dependent lifetime and emission intensity indicate that OQAO(mes)$_2$ is a TADF molecule. Triplet formation can be seen in the transient absorption (TA) spectrum of a 40 wt.% OQAO(mes)$_2$ in PMMA thin film, as shown in Figure 2c. A detailed description of TA measurements including deconvoluting the TA spectra into singlet and triplet components and their kinetics, i.e. the ISC rate constant, is provided in SI. As shown in Figure 2c, a long-lived species is observed at long wavelengths with a different spectral shape compared to S_1, which decays on a ns timescale. This longer-lived species is attributed to the triplet state formed via intersystem crossing (ISC) (see Figure 1a). Time resolved fluorescence was measured at both 560 nm and 620 nm using a thin film containing 35 wt.% OQAO(mes)$_2$ in PMMA. We found that the prompt fluorescence decay lifetimes varied at these different wavelengths (Figure S2b), which indicates decays of two different emissive species, singlet excitons and excimer. The emission lifetime is longer at 620 nm, originating from excimer. However, delayed emission at the two wavelengths showed identical lifetimes (see Figure S2c), indicating that the delayed fluorescence is dominated by the triplet kinetics, rather than excimer or singlet.

View Article Online
DOI: 10.1039/D3TC02133E

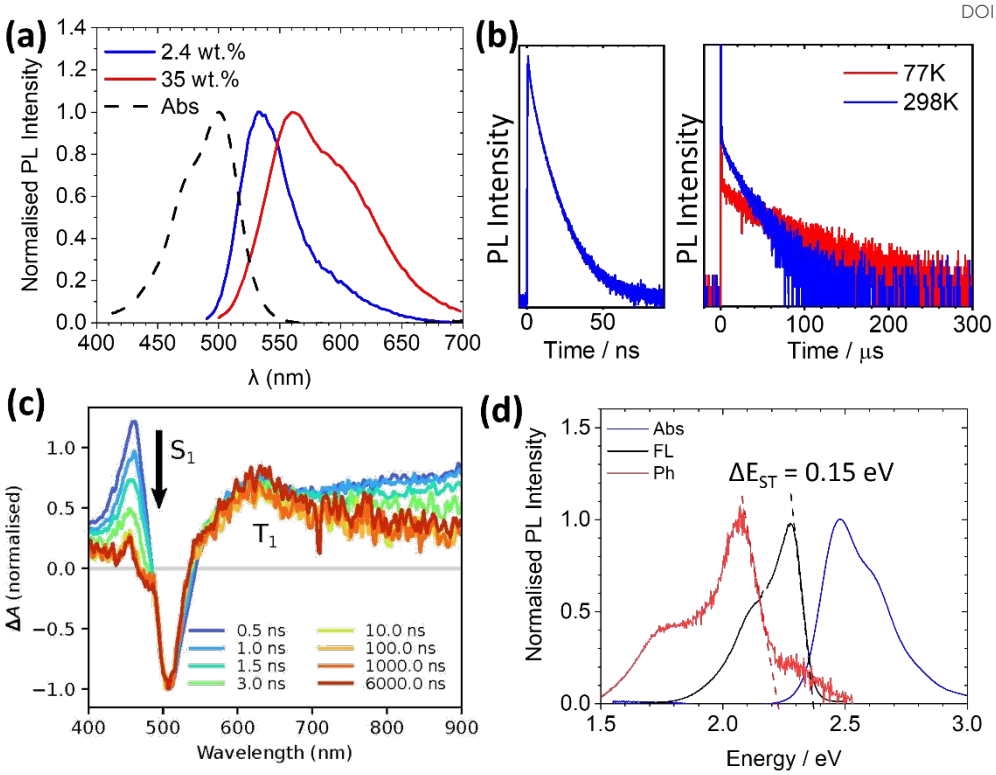

Figure 2. (a) Absorption and emission of OQAO(mes)$_2$-doped PMMA films at two doping concentrations, (b) prompt and delayed emission decays (logarithmic scale) at the 35 wt.% doping, (c) transient absorption spectra of 40 wt.% OQAO(mes)$_2$ in PMMA thin film at different delay times, and (d) absorption (Abs), fluorescence (FL), and phosphorescence (Ph, 500 µs delay and 2 ms gate time) of 9.1 wt.% OQAO(mes)$_2$ in PMMA at 77K, excited at 470 nm.

We measured the emission spectra of OQAO(mes)$_2$ at different delay and gate times at 77K. Figure 2d shows the normalised emission spectra of 9.1 wt.% OQAO(mes)$_2$ in PMMA. Prompt and delayed emission at 10 µs exhibit identical spectral shape, while emission at much longer timescales (> 500 µs) is red-shifted by 0.15 eV. We assign the red-shifted emission at the longer timescale (> 500 µs) to phosphorescence and the difference between the onsets of the fluorescence and the phosphorescence spectra to ΔE_{ST} of 0.15 eV which is close to the reported ΔE_{ST} of OQAO (0.16 eV).[38] As can be seen in Figure 2d, overlap between S_1 or excimer and phosphorescence spectra is minimal. Unless otherwise noted, time-resolved emission from S_1 or excimer was measured near the peak of fluorescence, i.e., at 540 nm (2.30 eV). Hence prompt and delayed emission can be considered as purely from S_1 or excimer species, with no phosphorescence contributions.

Strong Exciton-Photon Interactions.

To demonstrate strong light-matter coupling in optical cavities, the thin film of OQAO(mes)$_2$ doped in PMMA was embedded in an optical cavity and the reflected spectrum was measured at different angles to the incident light (see Figure 3b). The raw angularly resolved reflection data of the negatively detuned cavities is shown in Figure S4. At all doping concentrations, 1−reflection peak shifts towards higher energies as angle of incidence is increased. In the case of the 2.4 and 4.8 wt.% samples, shift in 1−reflection is observed without any splitting whilst presenting a slight broadening of the spectrum around the exciton transition energy at 2.45 eV. On the other hand, at higher doping concentrations, clear splitting is observed for two vibronic transitions at 2.45 and 2.60 eV that was fitted using a coupled harmonic oscillator model given by Equation 1,

$$\begin{pmatrix} E_C & \Omega_1/2 & \Omega_2/2 \\ \Omega_1/2 & E_{X1} & 0 \\ \Omega_2/2 & 0 & E_{X2} \end{pmatrix} \begin{pmatrix} \alpha \\ \beta \\ \gamma \end{pmatrix} = E \begin{pmatrix} \alpha \\ \beta \\ \gamma \end{pmatrix} \quad \text{Eq. 1}$$

where E_c is the angle-dependent cavity energy, E_{x1} and E_{x2} are the two vibronic transitions of OQAO(mes)$_2$, and Ω_1 and Ω_2 are the Rabi-splitting energies around E_{x1} and E_{x2}, respectively. α, β, and γ are the Hopfield coefficients representing contribution of each photon and exciton component to the polariton branches. Three angularly dispersed polariton branches (UP, MP, and LP) are needed to best fit the angular reflection data. Rabi splitting of Ω_1 and Ω_2 between polariton branches for 35 wt.% doping is found to be 0.15 and 0.24 eV, respectively (fitting parameters are given in Table S1 in SI). Angular reflection spectra of 9.1 wt.% doped film could be fitted using a 2-component coupled harmonic oscillator model (equation S1), giving a Ω between LP and UP states of 0.10 eV (see Figure S5).

View Article Online
DOI: 10.1039/D3TC02133E

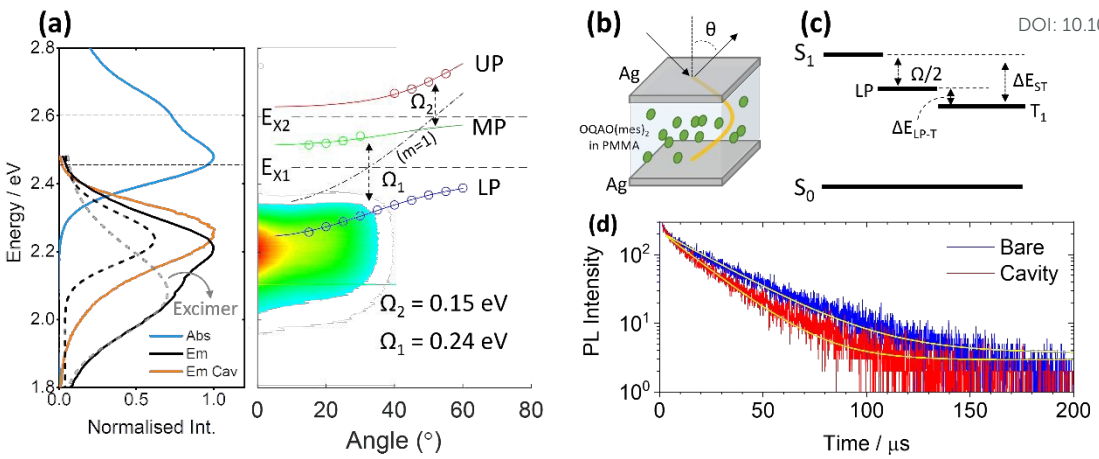

Figure 3. (a) Left panel: Absorption (Abs) and emission (Em) spectra of the 35 wt.% OQAO(mes)$_2$ in PMMA and emission of the film in a cavity (Em Cav). Deconvoluted spectra of the emission are shown as dashed lines, where the grey dashed line represents excimer emission. Right panel: Angular dispersion curves of 1-reflection and emission in the cavity. 1-reflection and emission peaks versus angle were fit with a coupled harmonic oscillator model (Eq.1). (b) Schematic illustration of the cavity thin film containing a OQAO(mes)$_2$-doped PMMA film. (c) Schematic energy diagram of the TADF under the strong exciton-photon coupling. (d) Delayed emission decays of the 35 wt.% OQAO(mes)$_2$ in PMMA with and without a cavity. Yellow lines are exponential fit to the decay curves.

The absence of splitting in 1-Reflection spectra at low doping concentrations (2.4 and 4.8 wt%) indicates that these films are in the weakly coupled regime. At higher concentrations (9.7 and 35 wt%), Rabi splitting is proportional to the square root of the number of molecules coupled with the cavity photon mode and inversely proportional to the mode volume (see Figure 3c). Assuming mode volumes for both samples were identical for similar cavity thickness, the twice as high value of Rabi splitting for 35 wt.% doping compared to that of the 9.1 wt.% one is due to the larger number of the molecules (≈ 5 times) coupled to the cavity photon mode. Linewidths of E_{X1} and E_c are 0.13 and 0.2 eV, respectively. The Rabi splitting value of 0.24 eV at 35 wt.% doping implies that this cavity film is in the strong coupling regime and the energy of the LP branch is lower than the singlet energy state by 0.12 eV. This opens up an opportunity for RISC to be mediated by LP states. We found that the delayed fluorescence lifetime of the cavity film (~ 18 μs) is decreased by 30% compared to that of the bare film (~ 26 μs) as shown in Figure 3d, indicating change in TADF photophysics.

TADF Photophysics in Optical Cavities.

Angle-resolved photoluminescence (PL) was performed to investigate from which energy state light is emitted in the cavity thin films. As can be seen in Figure 3a, the emission at approximately 2.2 eV shifts

View Article Online
DOI: 10.1039/D3TC02133E

towards higher energy with increasing angle, coinciding with the angularly dispersed LP state energy. Importantly, the emission spectrum of the cavity film shows reduced excimer emission as can be seen in Figure 3a. At 35 wt.% doping, the emission peak is blue shifted by 12 nm and the emission spectrum linewidth is significantly narrower by approximately 60% from 92 nm (bare) to 55 nm (cavity). This result is consistent with the report by Mony *et al.* who showed that emission from aggregation-induced molecular trap states can be suppressed by placing a TADF molecule in cavities and tuning/detuning the cavity photon energy.[35] This leads to an interesting implication that under strong coupling conditions, colour purity of light emitting dyes can be improved. Note that the sharpening of the emission bandwidth in a cavity thin film can also originate from cavity filtering effect. The emission bandwidth narrowing observed here is much larger than possible from cavity filtering effect (Figure S6).

The emission from the LP states with less excimer emission suggests that energy transfer from S_1 to the LP is efficient. Georgiou *et al.* have previously shown that energy transfer between a donor and an acceptor can be mediated efficiently via middle polariton branches, resulting in LP emission (with dominant acceptor character due to its lower lying exciton energy states compared to that of the donor) after exclusively exciting the donor species.[39] Our cavity thin film shows emission from LP states regardless of the excitation wavelengths (Figure S6). This suggests efficient energy transfer from higher polariton/exciton branches to the LP states, largely mitigating excimer emission. To identify if delayed emission is also from the same LP state, we measured delayed/gated emission of the same sample with the same excitation conditions. Figure S7 shows that the prompt and the delayed emission of the 35 wt.% cavity are similar in shape with a slight red shift observed for the delayed emission probably due to minor contribution of excimer emission that persists. However, both delayed and prompt emission are narrower and blue-shifted in the cavity compared to the broader emission of the bare film that is dominated by excimer emission, suggesting that the LP states are responsible for both prompt and delayed emission in the cavity.

Given that the energy of the LP states is lower than the singlet state by ≈0.12 eV, we next investigated the role of LP states on RISC dynamics. We fitted the emission decays of the cavity and the bare films using a kinetic model (see SI) and calculated k_{RISC}. This model considers rate constants of ISC and S_1-S_0 transition determined using TA spectra of thin films and the rate constants of unknown T_1-S_0 transition with two extreme scenarios. Figure 4a shows the k_{RISC} of the bare and the cavity films at multiple doping concentrations. Their emission decay curves can be seen in Figure S8. In the bare cases, k_{RISC} increases with increasing concentration. This increase in k_{RISC} may be due to the decrease in energy of aggregate states, consistent with the bathochromic shifts in emission spectra as shown in Figure 1 and S1, which lowers the activation energy of RISC. The observed increase in k_{RISC} with increasing concentration could also be explained by bimolecular processes such as triplet-triplet annihilation, rather than a change in the k_{RISC} alone. No fluence dependence was observed in the delayed emission lifetime, making bimolecular process unlikely. Moreover, when bimolecular triplet decay is included, the model is unable to reproduce the data without also changing k_{RISC} (see Figure S14). So we conclude that the change in delayed emission lifetime with concentration must at least be partially due to increasing $k_{RISC,}$ if not entirely.

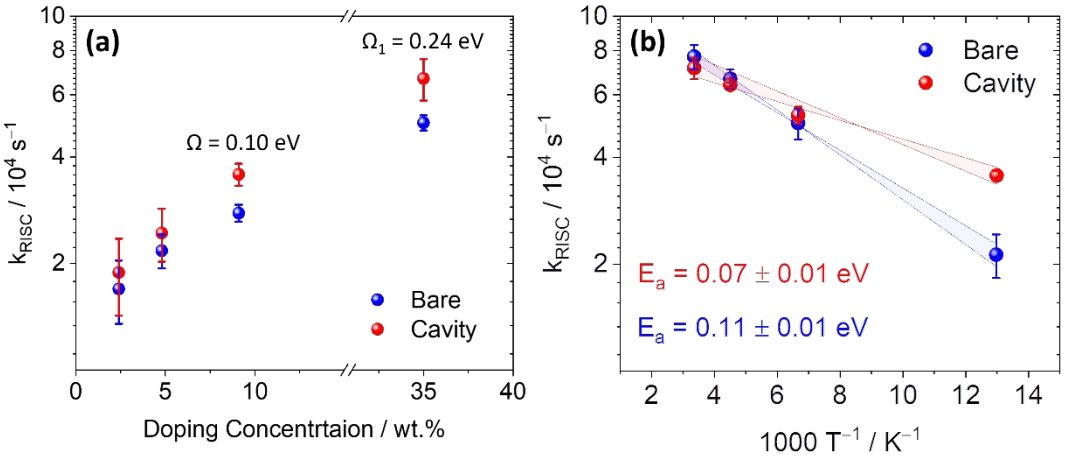

Figure 4. (a) k_{RISC} versus doping concentration and (b) k_{RISC} versus 1000/T of 35 wt.% OQAO(mes)$_2$ in PMMA with and without cavity. Emission decays were measured at 540 nm.

We found that k_{RISC} between cavity and bare films for 2.4 and 4.8 wt.% doping is the same within error. At higher concentrations, k_{RISC} is enhanced by 29% and 33% for the 9.1 wt.% and 35 wt.% doping, respectively, from bare to cavity film cases. We attribute this enhancement to the faster RISC from triplets to the LP states due to lower effective energetic barrier $\Delta E_{LP\text{-}T}$ (i.e. energy gap between LP and T_1 states) compared to ΔE_{ST} in the bare thin film (Figure 2c). This is consistent with the report by Stranius *et al*. who have shown that even in a phosphor material that is known to have ineffective RISC, k_{RISC} is enhanced when placed in an optical cavity. They attributed this to lower effective ΔE_{ST} (that is $\Delta E_{LP\text{-}T}$) by 118 meV in the strong coupling regime that resulted in a four-fold decrease in the phosphorescence decay lifetime.[32] To examine if the lower $\Delta E_{LP\text{-}T}$ is responsible for the enhancement in k_{RISC}, we further measured delayed emission decays at different temperatures and fit them using a kinetic model to determine k_{RISC} as a function of temperature (Figure 4b). The raw emission decay spectra can be seen in Figure S9 and the k_{RISC} values are shown in Table S4. By fitting the k_{RISC} at different temperatures using an Arrhenius equation, the slope of the fit gave us the E_a for RISC. E_a of the cavity thin film is indeed lower than that of the bare film by ≈ 2 kT. Note that a faster delayed fluorescence can also be partially explained by enhancement in the singlet decay rate (k_S) due to the Purcell effect and/or quenching of excited states at the metal surfaces. We expect the Purcell effect to be small due to the low Q factor of the Ag cavities used in this study. Regardless, to account for this effect, we modelled emission dynamics using singlet excited state lifetimes obtained from the prompt emission of cavity films on and off resonance, as shown in the SI. While our modelling shows that a larger k_S does result in an accelerated delayed fluorescence, this effect is not sufficient to account for the observed delayed fluorescence in cavities without also increasing k_{RISC} in the case of bare films, particularly at low temperatures. This suggests that the Purcell effect or metal quenching is not solely responsible for the k_S enhancement and that the strong coupling is playing a role for the enhanced delayed emission lifetimes in the cavities.

View Article Online
DOI: 10.1039/D3TC02133E

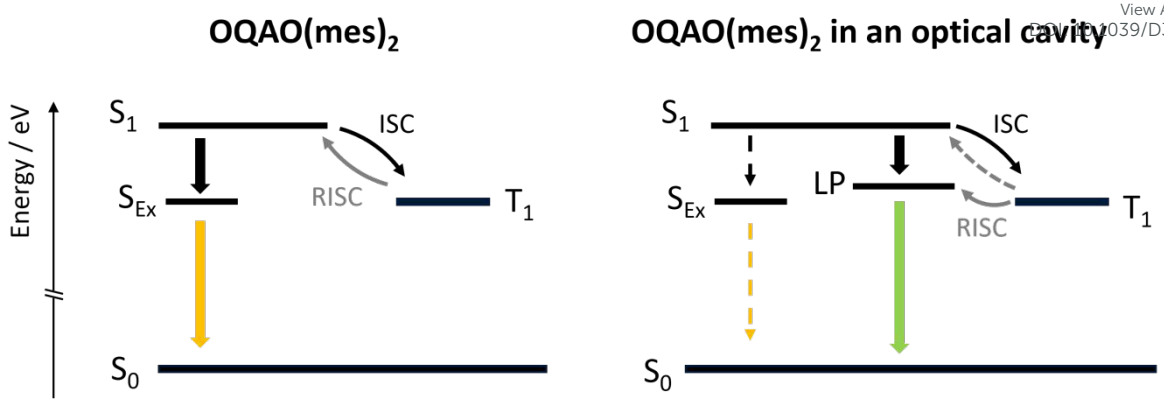

Figure 5. Schematic model of TADF in OQAO(mes)$_2$ with (left) and without the cavity (right) showing radiative decay from the singlet states. S_{Ex} and (R)ISC represent excimer energy states and the (reverse) intersystem crossing, respectively. Direct relaxation from S_1 and T_1 states to S_0 is omitted for clarity. Dotted lines depict reduced transition strengths.

We postulate that emission in the cavities occurs primarily from the LP states (Figure 5) due to efficient energy transfer from singlet states evidenced by the blue shift of the emission spectrum and a narrow emission linewidth compared to the broader excimer emission spectrum dominant in bare thin films. Photoluminescence quantum yield (PLQY) measurements of the bare thin films show more than a threefold decrease from 54% to 17% with increasing doping concentrations compared to the change in PLQY for cavity thin films that is relatively smaller (Figure S10). This indicates that the contribution from aggregation-induced non-radiative decay observed in bare films as a function of doping concentration is lessened by energy transfer to the LP states. Please note, here we only draw qualitative comparisons between PLQY of bare and cavity thin films. A quantitative comparison of PLQY in cavity thin films is difficult due to several factors such as outcoupling of light, reflection from Ag mirrors, cavity filtering effect, and light trapping due to surface plasmon modes.[40] A comprehensive set of measurements of incident, reflected, and transmitted light for prompt and delayed components as a function of cavity detuning supported by transfer matrix simulations and time-resolved spectroscopy will help draw quantitative comparisons,[41, 42] and follow-up work will focus on exploring these research directions.

The enhanced k_{RISC} in the cavity observed is attributed to the lower E_a, originating from the ΔE_{LP-T} compared to the ΔE_{ST} of bare OQAO(mes)$_2$. We do not rule out the role of dark states on RISC. The

View Article Online
DOI: 10.1039/D3TC02133E

difference between the E_a reduction value and the observed Rabi splitting in our MR-TADF system implies that its likely RISC photophysics involves dark states. Eizner *et al* found that in their donor-acceptor TADF dye 3DPA3CN, k_{RISC} was independent of the degree of Rabi splitting and argued that RISC through dark states can dominate emission.[33] Unlike donor-acceptor based TADF dyes such as 3DPA3CN dyes, MR-TADF systems are designed to have electronegative atom arrangements in their molecular structure that yield sharper emission and smaller stokes shifts. We infer that this difference in molecular structure is linked to the observation of k_{RISC} enhancement observed in MR-TADF system. Given the recent advances in using 2D white light spectroscopy and Redfield theory[42] to study energy transfer dynamics and dark state populations in optical cavities, we anticipate a comparative study between traditional donor-acceptor and MR-TADF systems using such techniques will be an interesting direction for future work.

CONCLUSION

We have demonstrated that excimer emission in an MR-TADF system can be effectively supressed under strong light-matter coupling regime. We report the synthesis of a new MR-TADF dye, (OQAO(mes)$_2$) that shows a ΔE_{ST} value of ≈ 0.15 eV. We can vary Rabi splitting as function of dye loading concentration in PMMA matrix achieving values up to 0.24 eV at 35 wt.% dye loading, enabling us to lower the effective ΔE_{ST} by ≈ 0.12 eV. We show that excimer emission is suppressed in the strong coupling regime due to efficient energy transfer to the LP states evidenced by strong LP emission. We observe that k_{RISC} is enhanced by 33% in optical cavities due to the lowering of the RISC activation energy, E_a by ≈2kT compared to bare thin films. This work highlights that aggregation-induced excimer emission that negatively impacts the emission quantum yield and colour purity of OLEDs can be controlled by strong light-matter coupling, demonstrating the potential benefit of optical cavities in OLED and organic semiconductor lasing applications.

EXPERIMENTAL

Chemicals and Materials.

View Article Online
DOI: 10.1039/D3TC02133E

2-propanol (Aldrich), Acetone (Aldrich), and D.I water were used to clean glass microscope slides (1 – 1.2 mm thick, pathology grade, LIVINGSTONE) for substrates. Chlorobenzene (anhydrous, 99.8%, Aldrich) was used to dissolve $OQAO(mes)_2$ and poly(methyl methacrylate) (PMMA, Mw=95,000, Aldrich). Ag pellets (99.99%, Kurt J. Lesker) were used on a tungsten boat (Kurt J. Lesker) for vacuum thermal evaporation for cavity mirrors. The synthesis of $OQAO(mes)_2$ is detailed in the SI (pages S14 – S26).

Thin Film Fabrication.

Thin film samples were prepared using a spin-coating method. Glass slides cut to be 2.5 x 2.5 cm^2 were used as substrates after three steps of solvent cleaning using D.I. water, isopropanol, and acetone, followed by UV-ozone cleaning for 10 min. Differently concentrated $OQAO(mes)_2$ solutions in chlorobenzene were separately prepared from the PMMA solution (40 mg mL^{-1} in chlorobenzene) and mixed on a hotplate set to 50 ˚C with stirring the solutions. Solutions were drop-casted at 50 ˚C while spinning at different spin speed (ranging from 2000 rpm to 5000 rpm with 1 sec ramp time) on a spin coater depending on the target thickness of the film. The thickness of the samples was measured using a surface profilometer (Dektak 150), resulting in thicknesses of around 120 nm (m = 1).

The active layer of the cavity films was prepared using the same method described in the above paragraph. 25 nm Ag mirrors sandwiching the active layer were deposited before and after the spin-coating by the thermal evaporation method under vacuum at the rate of 1 A/s.

Optical Measurements.

Absorption spectra of the thin films were recorded using a UV-vis spectrometer (Cary 60, Agilent), scanning from 300 nm to 800 nm. Emission spectra and the lifetimes were measured using a time-correlated single photon counting (TCSPC) setup (Deltaflex, HORIBA) under vacuum. Excitation was mostly at 450-470 nm using a white-light continuum lasers decorated with a monochromator or

View Article Online
DOI: 10.1039/D3TC02133E

bandpass filters (NKT SuperK Extreme, NKT Compact). Slit sizes for the photodetector was adjusted between 8 nm to 16 nm depending on the signal magnitudes.

Angular reflectometry was performed using a home-built setup consisting of a white light (NKT SuperK Compact, running at 22kHz) as an excitation light source and a spectrometer (FLAME, OceanOptics). Cavity samples were mounted on a rotational state aligned with the white light source and the reflected light was collected using an integrating sphere fibre-coupled to the spectrometer. Integrating time was 100 ms with averaging 50 spectra.

Angular PL measurements were performed using a home-made setup. Cavity devices were fixed onto a clamp holder and excited using a monochromatic light source (NKT SuperK Extreme), exciting the samples at 470 nm. Emission spectra were recorded with a fibre-coupled collimator on a rotating stage. Spectra were taken from 0 degree to 55 degrees on the same spectrometer used for the angular reflection measurement.

Transient absorption measurements were performed on a commercial nanosecond-timescale TA spectrometer (Ultrafast systems, EOS). The pump pulse was a 355 nm pulse at 1 kHz repetition rate (Innolas) with a spot size of 2.4 mm at the sample and with polarization rotated to magic angle relative to the probe pulse. The probe pulse was generated from a photonic crystal fibre based supercontinuum laser (Ultrafast systems, EOS), split into a signal and reference beam, and focused onto the sample with a 0.1 mm FWHM spot size.

Gated spectra and QY.

Gated spectra were measured using the phosphorescence mode and 470 nm excitation on a fluorescence spectrometer (Cary Eclipse, Agilent) equipped with an accessory for time-resolved luminescence measurements.

View Article Online
DOI: 10.1039/D3TC02133E

Absolute photoluminescence quantum yield (PLQY) measurements upon 470 nm excitation were performed using a fluorimeter with an integrating sphere accessory (Fluorog-3/F3018, Horiba John Yvon). All spectra were recorded with photon counts within the linear response range of the detector, and were corrected for light source noise, wavelength sensitivity and filter transmittance.

AUTHOR CONTRIBUTION

IC, WWHW, and GL conceived the idea and designed the experiments. IC prepared the samples, performed absorption, emission, angular reflectometry, angular emission, and time-resolved emission measurements, and analysed the data. ANS performed the transient absorbance measurements, analysed the data, and modelled the photophysics. PR performed the gated emission and PLQY measurements. WJK synthesised and characterised the $OQAO(mes)_2$ molecule. WWHW and KPG supervised the work of WJK and PR, respectively. GL supervised the work of IC and ANS and directed the entire study. IC, ANS, and GL wrote the manuscript with input from all co-authors.

CONFLICTS OF INTEREST

The authors declare there is no competing financial interest.

ACKNOWLEDGEMENTS

This work was supported by the Australian Research Council Centre of Excellence in Exciton Science (funding grant number CE170100026).

REFERENCES

1. M. A. Baldo, C. Adachi and S. R. Forrest, *Physical Review B*, 2000, **62**, 10967.
2. S. Reineke, K. Walzer and K. Leo, *Physical Review B*, 2007, **75**, 125328.
3. H. Van Eersel, P. Bobbert, R. Janssen and R. Coehoorn, *Applied Physics Letters*, 2014, **105**, 156_151.
4. Q. Wang, I. W. Oswald, M. R. Perez, H. Jia, B. E. Gnade and M. A. Omary, *Advanced Functional Materials*, 2013, **23**, 5420-5428.

5. M. Hasan, A. Shukla, V. Ahmad, J. Sobus, F. Bencheikh, S. K. McGregor, M. Mamada, C. Adachi, S. C. Lo and E. B. Namdas, *Advanced Functional Materials*, 2020, **30**, 2000580.
6. A. Niwa, S. Haseyama, T. Kobayashi, T. Nagase, K. Goushi, C. Adachi and H. Naito, *Applied Physics Letters*, 2018, **113**, 083301.
7. H. Uoyama, K. Goushi, K. Shizu, H. Nomura and C. Adachi, *Nature*, 2012, **492**, 234-238.
8. F. B. Dias, T. J. Penfold and A. P. Monkman, *Methods and applications in fluorescence*, 2017, **5**, 012001.
9. S. Madayanad Suresh, D. Hall, D. Beljonne, Y. Olivier and E. Zysman-Colman, *Advanced Functional Materials*, 2020, **30**, 1908677.
10. T. Hatakeyama, K. Shiren, K. Nakajima, S. Nomura, S. Nakatsuka, K. Kinoshita, J. Ni, Y. Ono and T. Ikuta, *Advanced Materials*, 2016, **28**, 2777-2781.
11. K. Matsui, S. Oda, K. Yoshiura, K. Nakajima, N. Yasuda and T. Hatakeyama, *Journal of the American Chemical Society*, 2018, **140**, 1195-1198.
12. Y. Kondo, K. Yoshiura, S. Kitera, H. Nishi, S. Oda, H. Gotoh, Y. Sasada, M. Yanai and T. Hatakeyama, *Nature Photonics*, 2019, **13**, 678-682.
13. H. J. Kim and T. Yasuda, *Advanced Optical Materials*, 2022, **10**, 2201714.
14. I. S. Park, K. Matsuo, N. Aizawa and T. Yasuda, *Advanced Functional Materials*, 2018, **28**, 1802031.
15. Y. Zhang, D. Zhang, J. Wei, X. Hong, Y. Lu, D. Hu, G. Li, Z. Liu, Y. Chen and L. Duan, *Angewandte Chemie*, 2020, **132**, 17652-17656.
16. Y. Xu, Z. Cheng, Z. Li, B. Liang, J. Wang, J. Wei, Z. Zhang and Y. Wang, *Advanced Optical Materials*, 2020, **8**, 1902142.
17. K. Stavrou, A. Danos, T. Hama, T. Hatakeyama and A. Monkman, *ACS Applied Materials & Interfaces*, 2021, **13**, 8643-8655.
18. F. Huang, X.-C. Fan, Y.-C. Cheng, H. Wu, Y.-Z. Shi, J. Yu, K. Wang, C.-S. Lee and X.-H. Zhang, *Materials Horizons*, 2022, **9**, 2226-2232.
19. J. Birks, *Reports on progress in physics*, 1975, **38**, 903.
20. J. M. Lim, P. Kim, M.-C. Yoon, J. Sung, V. Dehm, Z. Chen, F. Würthner and D. Kim, *Chemical Science*, 2013, **4**, 388-397.
21. T. Ye, R. Singh, H.-J. r. Butt, G. Floudas and P. E. Keivanidis, *ACS Applied Materials & Interfaces*, 2013, **5**, 11844-11857.
22. Z. Chen, V. Stepanenko, V. Dehm, P. Prins, L. D. Siebbeles, J. Seibt, P. Marquetand, V. Engel and F. Würthner, *Chemistry–A European Journal*, 2007, **13**, 436-449.
23. C. Adachi and A. S. Sandanayaka, *CCS Chemistry*, 2020, **2**, 1203-1216.
24. L.-S. Cui, A. J. Gillett, S.-F. Zhang, H. Ye, Y. Liu, X.-K. Chen, Z.-S. Lin, E. W. Evans, W. K. Myers and T. K. Ronson, *Nature Photonics*, 2020, **14**, 636-642.
25. N. Aizawa, Y.-J. Pu, Y. Harabuchi, A. Nihonyanagi, R. Ibuka, H. Inuzuka, B. Dhara, Y. Koyama, K.-i. Nakayama and S. Maeda, *Nature*, 2022, **609**, 502-506.
26. D. G. Baranov, M. Wersall, J. Cuadra, T. J. Antosiewicz and T. Shegai, *Acs Photonics*, 2018, **5**, 24-42.
27. L. Shi, T. Hakala, H. Rekola, J.-P. Martikainen, R. Moerland and P. Törmä, *Physical review letters*, 2014, **112**, 153002.
28. S. A. Guebrou, C. Symonds, E. Homeyer, J. Plenet, Y. N. Gartstein, V. M. Agranovich and J. Bellessa, *Physical Review Letters*, 2012, **108**, 066401.
29. S. Hou, M. Khatoniar, K. Ding, Y. Qu, A. Napolov, V. M. Menon and S. R. Forrest, *Advanced Materials*, 2020, **32**, 2002127.
30. D. M. Coles, N. Somaschi, P. Michetti, C. Clark, P. G. Lagoudakis, P. G. Savvidis and D. G. Lidzey, *Nature materials*, 2014, **13**, 712-719.
31. X. Zhong, T. Chervy, L. Zhang, A. Thomas, J. George, C. Genet, J. A. Hutchison and T. W. Ebbesen, *Angewandte Chemie*, 2017, **129**, 9162-9166.
32. K. Stranius, M. Hertzog and K. Börjesson, *Nature Communications*, 2018, **9**, 2273.

33. E. Eizner, L. A. Martínez-Martínez, J. Yuen-Zhou and S. Kéna-Cohen, *Science Advances*, 2019, **5**, eaax4482.
34. Y. Yu, S. Mallick, M. Wang and K. Börjesson, *Nature communications*, 2021, **12**, 3255.
35. J. r. Mony, Y. Yu, C. Schäfer, S. Mallick, K. Kushwaha and K. Börjesson, *The Journal of Physical Chemistry C*, 2022, **126**, 7965-7972.
36. R. P. Sabatini, B. Zhang, A. Gupta, J. Leoni, W. W. Wong and G. Lakhwani, *Journal of Materials Chemistry C*, 2019, **7**, 2954-2960.
37. R. Chikkaraddy, B. De Nijs, F. Benz, S. J. Barrow, O. A. Scherman, E. Rosta, A. Demetriadou, P. Fox, O. Hess and J. J. Baumberg, *Nature*, 2016, **535**, 127-130.
38. S.-N. Zou, C.-C. Peng, S.-Y. Yang, Y.-K. Qu, Y.-J. Yu, X. Chen, Z.-Q. Jiang and L.-S. Liao, *Organic Letters*, 2021, **23**, 958-962.
39. K. Georgiou, P. Michetti, L. Gai, M. Cavazzini, Z. Shen and D. G. Lidzey, *ACS Photonics*, 2018, **5**, 258-266.
40. R. Meerheim, M. Furno, S. Hofmann, B. Lüssem and K. Leo, *Applied Physics Letters*, 2010, **97**.
41. D. Ballarini, M. De Giorgi, S. Gambino, G. Lerario, M. Mazzeo, A. Genco, G. Accorsi, C. Giansante, S. Colella and S. D'Agostino, *Advanced Optical Materials*, 2014, **2**, 1076-1081.
42. M. Son, Z. T. Armstrong, R. T. Allen, A. Dhavamani, M. S. Arnold and M. T. Zanni, *Nature Communications*, 2022, **13**, 7305.